Theory of excitonic complexes in gated WSe_2 quantum dots

Daniel Miravet,[1,*] Ludmiła Szulakowska,[1] Maciej Bieniek,[2] Katarzyna Sadecka,[1,2] Marek Korkusiński,[1,3] and Paweł Hawrylak[1]

[1]*Department of Physics, University of Ottawa, Ottawa, K1N 6N5, Canada*

[2]*Institute of Theoretical Physics, Wrocław University of Science and Technology, Wybrzeże Wyspiańskiego 27, 50-370 Wrocław, Poland*

[3]*Quantum and Nanotechnologies Research Centre, National Research Council of Canada, Ottawa, Ontario, K1A 0R6, Canada*

(Received 24 June 2024; revised 12 November 2024; accepted 15 November 2024; published 4 December 2024)

We present here a theory of excitonic complexes in gated WSe_2 quantum dots (QDs). The QD gate potential causes type-II band alignment, i.e., electrostatically confines holes and repels electrons, or vice versa. Hence, the confinement of excitons involves a delicate balance of the repulsion of electrons by the gate potential with the attraction by the Coulomb potential of the hole localized in the QD. We present a theory of neutral excitonic complexes within a gated WSe_2 QD, considering spin, valley, electronic orbitals, and many-body interactions. We analyze how the electron-hole attraction depends on a range of parameters, such as screened Coulomb interaction, strength of confinement of holes, and repulsion of electrons. Using an atomistic tight-binding model, we compute valence and conduction band states within a computational box comprising over 1 million atoms with applied gate potential. The gate potential is split into a fictitious type-I potential which attracts both the electron and hole and a correction repelling the electron only. The atomistic wave functions are then used to calculate direct and exchange Coulomb matrix elements for a fictitious type-I QD and to obtain a spectrum of interacting electron-hole pairs. Next, the effect of repulsive potential, pulling away the electron from the valence hole, is included in the excitonic basis. This allows us to determine whether electron-hole pairs are sufficiently attracted to overcome electron repulsion by the confinement potential. Finally, we compute the dipole transition between hole and electron states to obtain the absorption spectrum.

DOI: 10.1103/PhysRevB.110.235404

I. INTRODUCTION

In a semiconductor, absorption of a single photon generates a single exciton, composed of a single electron-hole pair. Hence, detecting an exciton is equivalent to detecting a single photon. Gated quantum dots (QDs) enable precise manipulation and control of the number of either electrons or holes [1]. However, counting the number of excitons in gated QDs presents a nontrivial challenge, as the electron is repelled by the gate potential which confines the hole in the dot. Should a single exciton be confined in a gated QD, its presence could be detected in transport. The confinement of excitons in GaAs gated QDs has been investigated by Fujita *et al.* [2], Pioda *et al.* [3], and Schinner *et al.* [4]. In this paper, we provide a theory of strongly bound excitonic complexes in gated QDs within a single layer of two-dimensional (2D) materials, such as WSe_2. Such a theory is needed as gated QDs in WSe_2 are being developed [5,6] with potential application as polarization-resolved single photon detectors.

Transition metal dichalcogenides (TMDCs) such as WSe_2 have attracted interest due to their intriguing electronic, optical, and magnetic properties. These arise from strong electron-electron interactions and dimensionality lowering in a single atomic layer. Recent advancements in TMDCs, fabricated at the few-atomic-layer scale, have expanded our understanding of low-dimensional physics [5–18]. Unlike monolayer graphene, TMDCs possess a band gap, enabling optoelectronic devices [9,18–20].

TMDCs consist of transition metal atoms bonded to chalcogenide dimers. Their electronic and optical properties predominantly stem from the d orbitals of metal atoms [21–24]. The strong localization of these orbitals, combined with reduced screening in 2D, gives rise to pronounced correlation effects, ultimately leading to the formation of excitons with large binding energies [25–32].

The spin-orbit coupling (SOC) in TMDCs gives rise to distinct spin-dependent phenomena. Notably, WSe_2 stands out due to its substantial spin-orbit splitting ($\sim$500 meV) in the valence band (VB), distinguishing it from other TMDC materials [33,34]. Additionally, it is worth noting that, while the bottom of the conduction band (CB) in valleys K and $-K$ is predominantly composed of $m_d = 0$ orbitals, the top of the VB in valleys K and $-K$ primarily comprises $m_d = -2$ and $m_d = 2$ orbitals, respectively, indicating orbital asymmetry between the valleys [23].

Recent progress in graphene and TMDC materials, combined with lateral gating techniques [1], has enabled the fabrication of lateral finite size gated QDs [5,35–47]. By applying lateral metallic gates, electrons or holes can be laterally electrostatically confined, resulting in the creation of QD states [5,22,23,43–45,48–55] and strongly interacting many-particle complexes [24,56,57]. Excitons in gate-defined QDs in semiconductor quantum wells have been

*Contact author: dmiravet@uottawa.ca

successfully detected experimentally [2–4]. More recently, exciton confinement has also been demonstrated in $MoSe_2$ using one-dimensional [31] and zero-dimensional [32] electrostatic confinement techniques. In these systems, the electron-hole Coulomb attraction plays a critical role in offsetting the gate-induced repulsion of one of the charge carriers, facilitating exciton confinement.

Given these experimental developments, we present here a theory of excitons [25,58] in gated WSe_2 QDs [22,24] and predict a set of parameters involving spin, valley, topology, and many-body interactions for which an exciton can be created and confined in a type-II gated QD [5,40,47–49,51,59]. We describe our QD within a computational box containing >1 million atoms, employing a tight-binding microscopic Hamiltonian [27]. The gated QD is defined by applying lateral gates that result in a confining potential, which is attractive for holes and repulsive for electrons. By expanding the QD wave function in bulk band states, we obtain QD energy levels and wave functions, capturing the effects of confinement potential, size, valley, and spin [6,24].

To investigate excitonic states, we first construct the basis of electron-hole pairs and expand the exciton wave function in terms of these pairs. Using atomistic wave functions, we calculate the Coulomb matrix elements, which are crucial for determining whether electrons are sufficiently attracted by holes to overcome the repulsive gate potential acting on the electron. Instead of immediately solving for the real QD—which confines holes but repels electrons that reside outside a QD—we first determine exciton levels in an auxiliary QD, which confines both electrons and holes. We then introduce the electron-repelling potential and expand it in the basis of the exciton states of the auxiliary QD. This approach allows us to capture the delicate balance between the repulsive gate potential and the attractive Coulomb interaction between the electron and hole localized in the QD. Finally, we determine the confining potential and strength/screening of electron-electron interactions for which exciton is confined in a QD and can be detected in transport experiments.

The paper is organized as follows. In Sec. II, we describe the single-particle states in the gated WSe_2 QD, along with an overview of the formulation of the many-body problem and the computation of the dipole matrix elements. The phase diagram describing stable exciton as a function of confining potential strength and Coulomb interactions and resulting excitonic absorption spectrum are presented in Sec. III. The paper concludes with a summary and key findings in Sec. IV.

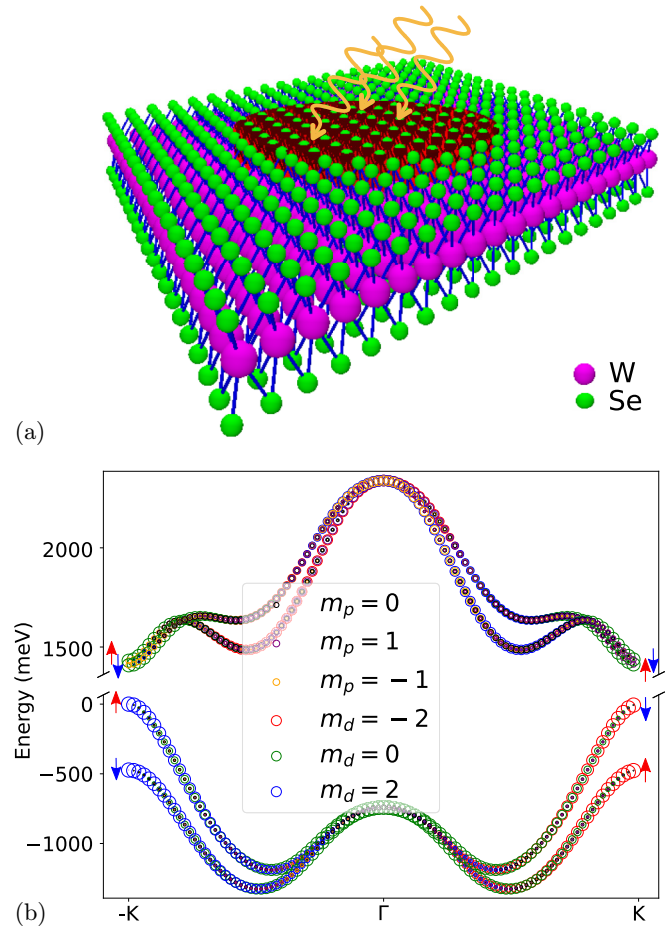

FIG. 1. (a) Schematic representation of the system showing a rhomboidal computational box with a quantum dot (QD) in the center. The yellow arrow represents the incident light to be absorbed by creating an electron-hole pair. (b) Highest-energy valence bands (VBs) and lowest-energy conduction bands (CBs) as a function of wave vector k over the path $-K \to \Gamma \to +K$. For the VB, the states in the $+K$ valley are composed mainly of $m_d = -2$ orbitals, while states in the $-K$ valley are composed primarily of $m_d = +2$ orbitals. On the other hand, the states in the CB $+K$ valley are composed primarily of $m_d = 0$ and $m_p = +1$ orbitals, while states in the $-K$ valley are composed primarily of $m_d = 0$ and $m_p = -1$ orbitals. The $+K$ and $-K$ points represent the global valley maxima (minima) of the valence (conduction) band.

II. MODEL

A. Tight-binding model

We follow here our earlier work on holes in gated WSe_2 QD [6,21,24]. We start with our computational box consisting of W and Se atoms arranged in a rhombus [see Fig. 1(a)]. By applying periodic boundary conditions, we obtain a set of allowed wave vectors $\vec{k}$. The wave functions of the computational rhombus at each wave vector $\vec{k}$ are constructed as a linear combination of Bloch functions on the tungsten and selenium atoms sublattices. We consider six such Bloch functions indexed by orbitals l ($l = 1, \ldots, 6$) corresponding to 3 m_d and 3 m_p orbitals:

$$\left|\phi^{p}_{\vec{k}\sigma}\right\rangle = \sum_{l=1}^{6} A^{p}_{\vec{k}\sigma,l} \left|\phi^{\text{even}}_{\vec{k},l}\right\rangle \otimes |\chi_\sigma\rangle, \tag{1}$$

where $|\chi_\sigma\rangle$ represents the spinor part of the wave function, and

$$\left|\phi^{\text{even}}_{\vec{k},l}\right\rangle = \frac{1}{\sqrt{N_{\text{UC}}}} \sum_{\vec{R}_l=1}^{N_{\text{UC}}} \exp(i\vec{k}\cdot\vec{R}_l)\varphi^{\text{even}}_{l}(\vec{r}-\vec{R}_l), \tag{2}$$

are Bloch functions constructed with orbitals $\varphi^{\text{even}}_{l}$, which are even with respect to the metal plane. Here, N_{UC} denotes the number of unit cells, and $\vec{R}_l$ defines the position of orbitals in the computational box. By diagonalizing the 6×6

bulk Hamiltonian [27], we obtain the even bulk energy bands $E^{\mathrm{p}}_{k\sigma}$ and wave functions $|\phi^{\mathrm{p}}_{k\sigma}\rangle$, where p is the band index. Figure 1(b) shows the energy $E^{p}_{k\sigma}$ of the highest even VB and lowest even CB along the path $-K \to \Gamma \to K$. It is important to note that the spin splitting Δ_{SOC} is opposite in these valleys, with a magnitude of ∼470 meV [33] for the VB and 50 meV for the CB. While the bottom of the CB in valleys K and $-K$ is mainly composed of $m_d = 0$ orbitals, the top of the VB in valleys K and $-K$ consists primarily of $m_d = -2$ and $m_d = 2$ orbitals, respectively.

B. Gate-defined quantum dot

In Ref. [24], it was shown that, by applying a confining Gaussian potential due to lateral gates $V_{\mathrm{QD}}(\vec{r}) = V_0 \exp(-r^2/R^2_{\mathrm{QD}})$, where $V_0 > 0$, to a single layer of WSe_2, a QD with confined hole states can be created, with R_{QD} denoting the QD radius. The single-particle Hamiltonian describing a particle in a WSe_2 QD can be expressed as the sum of the bulk computational box Hamiltonian H_{TB} and the confining potential V_{QD} [22]. The wave function $|\Phi^s\rangle$, associated with the state s, can be determined by solving the Schrödinger equation:

$$[H_{\mathrm{TB}} + V_{\mathrm{QD}}(\vec{r})]|\Phi^s\rangle = E^s|\Phi^s\rangle. \tag{3}$$

We expand QD wave function $|\Phi^s\rangle$ in terms of bulk states of the computational box, given by Eq. (1):

$$|\Phi^s\rangle = \sum_{\vec{k}} \sum_{p} \sum_{\sigma} B^{\mathrm{s,p}}_{\vec{k}\sigma} |\phi^{p}_{\vec{k}\sigma}\rangle, \tag{4}$$

where p runs over the highest-energy even VB and the lowest-energy even CB. Since we focus on the highest VB and lowest CB states, we apply a cutoff to the $\vec{k}$ points near K and $-K$ valleys by selecting vectors $\vec{k}$ that satisfy the condition $|\vec{k} \pm \vec{K}| < \eta|\vec{K}|$. This approach helps us focus on the relevant region of the reciprocal space. In this paper, we have maintained a fixed value of $\eta = 0.1$ throughout our calculations [24].

Then expanding the QD Hamiltonian in terms of the band states, we have

$$\begin{aligned}\hat{H} = \hat{H}_{\mathrm{TB}} &+ \sum_{\vec{k},\vec{q},\sigma} c^{\mathrm{VB}^\dagger}_{\vec{k},\sigma} c^{\mathrm{VB}}_{\vec{q},\sigma} \langle \phi^{VB}_{\vec{k}\sigma} | \hat{V}_{\mathrm{QD}} | \phi^{VB}_{\vec{q}\sigma} \rangle \\ &+ \sum_{\vec{k},\vec{q},\sigma} c^{\mathrm{CB}^\dagger}_{\vec{k},\sigma} c^{\mathrm{CB}}_{\vec{q},\sigma} \langle \phi^{\mathrm{CB}}_{\vec{k}\sigma} | \hat{V}_{\mathrm{QD}} | \phi^{\mathrm{CB}}_{\vec{q}\sigma} \rangle \\ &+ \sum_{\vec{k},\vec{q},\sigma} c^{\mathrm{VB}^\dagger}_{\vec{k},\sigma} c^{\mathrm{CB}}_{\vec{q},\sigma} \langle \phi^{\mathrm{VB}}_{\vec{k}\sigma} | \hat{V}_{\mathrm{QD}} | \phi^{\mathrm{CB}}_{\vec{q}\sigma} \rangle + \mathrm{H.c.}\end{aligned} \tag{5}$$

Here, the first term, diagonal, corresponds to the CB and VB energies of the tight-binding computational box Hamiltonian. The second and third terms denote the interaction between the QD-confining potential and the VB and CB states, respectively. The final term represents the coupling between CB and VB states induced by the confining potential.

Figure 2 schematically illustrates the effect of the confining potential. We can deplete some confined VB states by appropriately tuning the chemical potential or equivalently creating confined hole QD states. While the confined hole states are pushed into the band gap, the low-energy CB states are pushed away from the center of the QD and delocalized. As a consequence, the type-II-like electron-hole pairs are the most energetically favorable, with the hole confined within the QD and the electron outside of it. However, when Coulomb interaction is included, this picture changes due to the strong electron-hole attraction, which binds the electron to the hole in a type-I exciton state. This exciton is also strongly coupled to light because both electron and hole states are confined inside the QD. Therefore, we will focus on determining the parameters of the QD, the strength of the potential repelling an electron vs the strength of attraction by the hole in the formation of the type-I exciton bound in a QD.

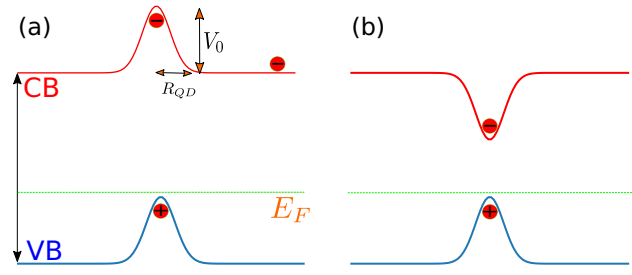

FIG. 2. (a) Schematic representation of the confinement in the quantum dot (QD) created by a gate potential. Confined states in the valence band are pushed into the gap, while states in the conduction band are pushed away from the gap. (b) Schematic representation of the auxiliary QD. The auxiliary potential confines both hole and electron states.

To artificially select CB states localized in the QD [see Fig. 2(b)], we subtract and add the term $\sum_{\vec{k},\vec{q},\sigma} c^{\mathrm{CB}^\dagger}_{\vec{k},\sigma} c^{\mathrm{CB}}_{\vec{q},\sigma} \langle \phi^{\mathrm{CB}}_{\vec{k}\sigma} | \hat{V}_{\mathrm{QD}} | \phi^{\mathrm{CB}}_{\vec{q}\sigma} \rangle$ in the Hamiltonian [Eq. (5)] confining and repelling electrons from the QD:

$$\begin{aligned}\hat{H} = \hat{H}_{\mathrm{TB}} &+ \sum_{\vec{k},\vec{q},\sigma} c^{\mathrm{VB}^\dagger}_{\vec{k},\sigma} c^{\mathrm{VB}}_{\vec{q},\sigma} \langle \phi^{\mathrm{VB}}_{\vec{k}\sigma} | \hat{V}_{\mathrm{QD}} | \phi^{\mathrm{VB}}_{\vec{q}\sigma} \rangle \\ &- \sum_{\vec{k},\vec{q},\sigma} c^{\mathrm{CB}^\dagger}_{\vec{k},\sigma} c^{\mathrm{CB}}_{\vec{q},\sigma} \langle \phi^{\mathrm{CB}}_{\vec{k}\sigma} | \hat{V}_{\mathrm{QD}} | \phi^{\mathrm{CB}}_{\vec{q}\sigma} \rangle \\ &+ \sum_{\vec{k},\vec{q},\sigma} c^{\mathrm{VB}^\dagger}_{\vec{k},\sigma} c^{\mathrm{CB}}_{\vec{q},\sigma} \langle \phi^{\mathrm{VB}}_{\vec{k}\sigma} | \hat{V}_{\mathrm{QD}} | \phi^{\mathrm{CB}}_{\vec{q}\sigma} \rangle + \mathrm{H.c.}, \\ &+ 2 \sum_{\vec{k},\vec{q},\sigma} c^{\mathrm{CB}^\dagger}_{\vec{k},\sigma} c^{\mathrm{CB}}_{\vec{q},\sigma} \langle \phi^{\mathrm{CB}}_{\vec{k}\sigma} | \hat{V}_{\mathrm{QD}} | \phi^{\mathrm{CB}}_{\vec{q}\sigma} \rangle.\end{aligned} \tag{6}$$

The first three lines of this Hamiltonian describe an auxiliary QD that confines both electrons and holes. while the last line is the correction (perturbation), which pulls only the electrons in the CB away from the QD. We first obtain the single-particle states for an auxiliary QD confining both holes and electrons and then compute confined exciton states by diagonalizing the many-body Hamiltonian in Sec. III B. This allows us to determine whether the repulsive electron potential can pull the electron from the bound exciton state:

$$\hat{H} = \hat{H}_{\mathrm{aux}} + \hat{V}_{\mathrm{corr}}. \tag{7}$$

Here,

$$\hat{H}_{\text{aux}} = \hat{H}_{\text{TB}} + \sum_{\vec{k},\vec{q},\sigma} c^{\text{VB}^\dagger}_{\vec{k},\sigma} c^{\text{VB}}_{\vec{q},\sigma} \langle \phi^{VB}_{\vec{k}\sigma} | \hat{V}_{\text{QD}} | \phi^{VB}_{\vec{q}\sigma} \rangle - \sum_{\vec{k},\vec{q},\sigma} c^{\text{CB}^\dagger}_{\vec{k},\sigma} c^{\text{CB}}_{\vec{q},\sigma} \langle \phi^{\text{CB}}_{\vec{k}\sigma} | \hat{V}_{\text{QD}} | \phi^{\text{CB}}_{\vec{q}\sigma} \rangle + \sum_{\vec{k},\vec{q},\sigma} c^{\text{VB}^\dagger}_{\vec{k},\sigma} c^{\text{CB}}_{\vec{q},\sigma} \langle \phi^{\text{VB}}_{\vec{k}\sigma} | \hat{V}_{\text{QD}} | \phi^{\text{CB}}_{\vec{q}\sigma} \rangle + \text{H.c.} \quad (8)$$

is the Hamiltonian for the auxiliary QD which confines electrons and holes, and

$$\hat{V}_{\text{corr}} = 2 \sum_{\vec{k},\vec{q},\sigma} c^{\text{CB}^\dagger}_{\vec{k},\sigma} c^{\text{CB}}_{\vec{q},\sigma} \langle \phi^{\text{CB}}_{\vec{k}\sigma} | \hat{V}_{\text{QD}} | \phi^{\text{CB}}_{\vec{q}\sigma} \rangle \quad (9)$$

is a correction that pulls the electron in CB away from the hole in a QD. In Sec. III A, we will determine the spectrum of this auxiliary QD as the first step toward the understanding of the original QD.

In numerical calculations, we employ a computational box containing $N_1 \times N_2 = 633 \times 633$ unit cells, corresponding to $3 \cdot N_1 \times N_2 = 1\,202\,067$ atoms. Periodic boundary conditions are enforced on the computational box, resulting in a discrete set of $\vec{k}$ points in reciprocal space.

C. Interactions

The optical properties of QDs are governed by excitonic complexes. We start here by computing excitons in the auxiliary QD, which requires the diagonalization of the many-body Hamiltonian in the space of electron-hole excitations:

$$H = \sum_i E^i c_i^\dagger c_i + \frac{1}{2} \sum_{i,j,k,l} \langle ij|V|kl\rangle c_i^\dagger c_j^\dagger c_k c_l - \sum_{i,j} \sum_{m \in \text{occup}} \langle im|V|mj\rangle c_i^\dagger c_j. \quad (10)$$

Here, E^i represents the energies of the auxiliary QD single-particle states, obtained by diagonalization of the Hamiltonian given by Eq. (8). The operator $c_i^\dagger$ (c_i) creates (annihilates) a particle in the auxiliary QD state i. The Coulomb matrix elements, denoted as $\langle ij|V|kl\rangle$, are expressed in terms of the auxiliary QD single-particle orbitals as

$$\langle ij|V|kl\rangle = \int d\vec{r}_1 \int d\vec{r}_2 \Phi^i(\vec{r}_1)^* \Phi^j(\vec{r}_2)^* V(\vec{r}_2 - \vec{r}_1) \times \Phi^k(\vec{r}_2) \Phi^l(\vec{r}_1), \quad (11)$$

where $\Phi^i(\vec{r}) = \langle \vec{r}|\Phi^i\rangle$, and V_C is the Coulomb potential $V_C = e^2/4\pi\epsilon\epsilon_0|\vec{r}_1 - \vec{r}_2|$, with e being the electron charge, ϵ_0 being the vacuum dielectric permittivity, and ϵ being the dielectric constant. The last term in Eq. (10) represents the interaction of the electron with the compensating background.

We approximate the ground state of the auxiliary QD as a single Slater determinant with all VB states occupied, denoted as $|\text{GS}\rangle = \Pi_{p \in \text{VB}} c_p^\dagger |0\rangle$. Subsequently, we construct the many-body excitations by generating all possible configurations of electron-hole pairs excited from the ground state with $S_z = 0$:

$$|X^\mu_{\text{aux}}\rangle = \sum_{p \in \text{VB}, q \in \text{CB}, \sigma_p = \sigma_q} A^\mu_{p,q} c_q^\dagger c_p |\text{GS}\rangle. \quad (12)$$

Here, the index μ enumerates the excitonic states, and $A^\alpha_{p,q}$ represents the expansion coefficients of the corresponding eigenvector.

D. Exciton in a QD

We now have a basis of excitonic states in an auxiliary QD and perturbation $\hat{V}_{\text{corr}}$, which pulls the electron in the CB away from the hole in a QD. The exciton spectrum $|X^\alpha\rangle$ of a gated QD can now be expanded in the basis of exciton states $|X^\mu_{\text{aux}}\rangle$ of the auxiliary QD:

$$|X^\alpha\rangle = \sum_\mu D^\alpha_\mu |X^\mu_{\text{aux}}\rangle. \quad (13)$$

Then the QD exciton states satisfy the equation:

$$E^{\text{aux}}_\mu D^\alpha_\mu + \sum_{\mu'} \langle X^\mu_{\text{aux}} | \hat{V}_{\text{corr}} | X^{\mu'}_{\text{aux}} \rangle D^\alpha_{\mu'} = E_\alpha D^\alpha_\mu. \quad (14)$$

Here, E^{aux}_α are auxiliary exciton energies, and $\langle X^\mu_{\text{aux}}|\hat{V}_{\text{corr}}|X^{\mu'}_{\text{aux}}\rangle$ is the effect of the repulsive potential acting on electrons in the CB only, pulling electrons away from the exciton levels localized in the QD, with a hole attracting the electron.

E. Absorption spectrum of auxiliary QD

To understand which excitonic states are optically active and contribute to true exciton spectrum, we compute the absorption spectrum of an auxiliary QD, $A(\omega)$, as a function of the photon energy ω. Here, $A(\omega)$ is computed using Fermi's golden rule as

$$A(\omega) = \sum_\mu |\langle X^\mu | P^\dagger | \text{GS}\rangle|^2 \delta(\omega - E_\mu + E_{\text{GS}}), \quad (15)$$

where E_{GS} is the energy of the initial state, and E_μ is the energy of the final excitonic state. The polarization operator $P^\dagger = \sum_{p,q} \delta_{\sigma_p,\sigma_q} \vec{\varepsilon}_0 \cdot \vec{D}_{qp} c_q^\dagger c_p$ creates a single pair excitation, $\vec{\varepsilon}_0$ denotes the polarization vector of the circularly polarized light, and the dipole elements $\vec{D}_{qp}$ are given by

$$\vec{D}_{qp} = \langle q|\vec{r}|p\rangle = \delta_{\sigma_p,\sigma_q} \sum_{\vec{R}_1,\vec{R}_2} \sum_{\vec{l}_1,\vec{l}_2} C^{q*}_{\vec{R}_1,l_1} C^{p}_{\vec{R}_2,l_2} \langle \varphi^{\text{even}}_{\vec{R}_1,l_1} | \vec{r} | \varphi^{\text{even}}_{\vec{R}_2,l_2} \rangle, \quad (16)$$

where $C^s_{\vec{R},l} = \sum_{\vec{k}} A^p_{\vec{k}\sigma,l} B^{\text{s,p}}_{\vec{k}\sigma} \exp(i\vec{k} \cdot \vec{R}_l)$, and

$$\langle \varphi^{\text{even}}_{\vec{R}_1,l_1} | \vec{r} | \varphi^{\text{even}}_{\vec{R}_2,l_2} \rangle = \int d\vec{r} \varphi^{\text{even}*}_{\vec{R}_1,l_1} (\vec{r} - \vec{R}_1 - \vec{\tau}_{l_1}) \vec{r} \times \varphi^{\text{even}}_{\vec{R}_2,l_2} (\vec{r} - \vec{R}_2 - \vec{\tau}_{l_2}). \quad (17)$$

III. DISCUSSION

A. Excitons in auxiliary QD

We obtain the energy levels and wave functions of the auxiliary QD by solving Eq. (8). In Fig. 3(a), we illustrate the one-particle levels for the auxilliary QD that confines

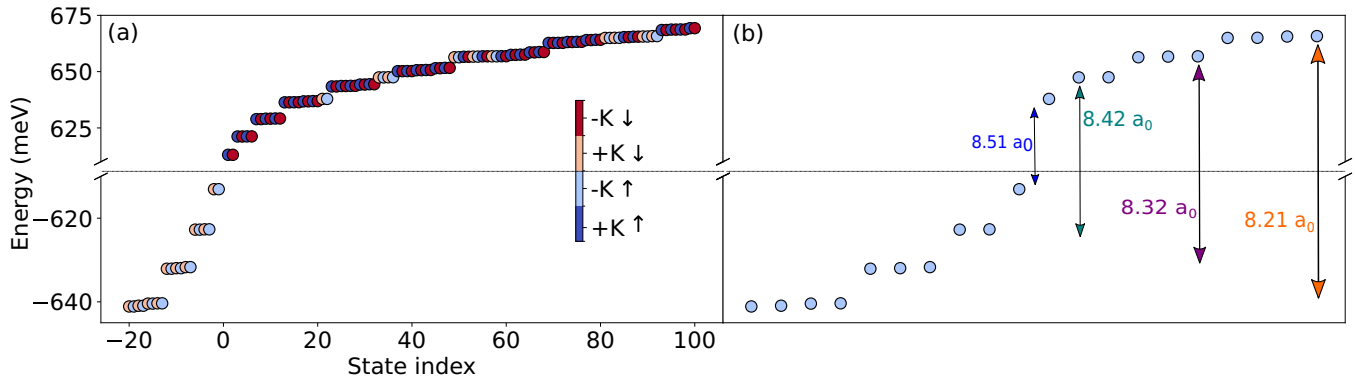

FIG. 3. Auxiliary quantum dot (QD) energy levels for $R_{QD} = 20\,\text{nm}$ and $V_0 = 100\,\text{meV}$. (a) The auxiliary QD energy levels. (b) The highest valence QD states and the conduction QD states with spin-up, localized in the $-K$ valley. The arrows represent the primary allowed transitions between different valence and conduction levels of the QD; the numbers represent the values of the dipole matrix elements of the transitions. The horizontal dashed line represents the Fermi level.

both electrons and holes. Each color represents different valley and spin combinations. The plot shows that the energy levels exhibit a distinctive grouping into shells, resembling the spectrum of a harmonic oscillator. Due to the significant SOC in the VB of WSe_2, the QD VB states exhibit spin locking, with spin-up states localized in the $-K$ valley and spin-down states in the $+K$ valley. Conversely, the SOC for the CB is relatively small, allowing for all spin and valley combinations within energy windows of 60 meV.

A consequence of the spin locking is that the lowest transitions in the QD are dark since the closest states in the CB are in opposite valleys or with opposite spin. The possible optically active transitions are to spin-up states localized in the $-K$ valley and spin-down states in the $+K$ valley. Figure 3(b) shows the highest valence QD states and the conduction QD state sharing the same spin for valley $-K$. The arrows in Fig. 3(a) represent the primary allowed transitions between the QD valence and conduction levels. The largest transitions occur between states with the same shell structure, such as s to s or p to p, while dipole transitions between states in different shells are $\sim$1 order of magnitude smaller. In Fig. 4, we depict the absorption spectrum as a function of photon energy for the auxiliary QD that confines both electrons and holes. The vertical black lines correspond to energies of excitonic states, while the red line represents the absorption strength for the optically active states.

The upper panel illustrates the noninteracting exciton spectrum, which can be understood with the help of Fig. 3. The lowest exciton state is dark, involving transitions between valence and conduction states in the s shells. We observe four peaks with increasing heights, representing transitions from valence states within equivalent shells to conduction states. The peak heights increase for higher-energy transitions due to the increased degeneracy of the shells. Smaller peaks represent inter-shell transitions with smaller dipole elements.

Moving to the center panels, we incorporate the electron-hole interaction effect, without considering scattering between different excitonic configurations. The peaks shift to higher energies due to the exchange self-energy compensated partially by electron-hole attraction.

The lower panel in Fig. 4 displays the exciton absorption spectrum, including all terms in the electron-electron interaction matrix elements. Here, we observe a more significant redistribution of peak heights, given by correlations between different excitonic configurations. Additionally, the brightest peak experiences a redshift. The lowest-energy peak corresponds to a correlated state, wherein the bright transition between the s-shells contributes $\sim$30%.

B. QD excitonic spectrum

Now we will discuss the original QD with a confining potential that confines holes but repels electrons. Using the auxiliary QD excitonic states, we will solve Eq. (14). By doing this, we are including the correction represented by Eq. (9).

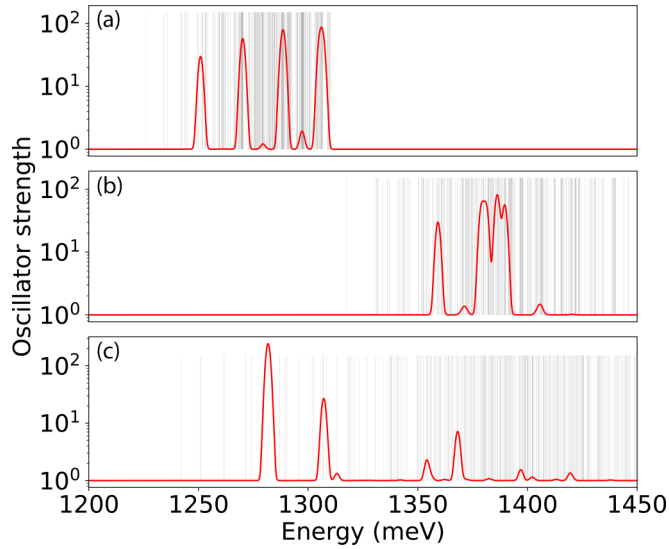

FIG. 4. Low-energy absorption spectrum for the auxiliary quantum dot (QD) with $R_{QD} = 20\,\text{nm}$, $V_0 = 100\,\text{meV}$, and $\epsilon = 3.9$. (a) shows the single-particle picture, (b) includes self-energy and vertex corrections on top of it, and (c) also allows for the scattering of configurations. The broadening has been added by hand.

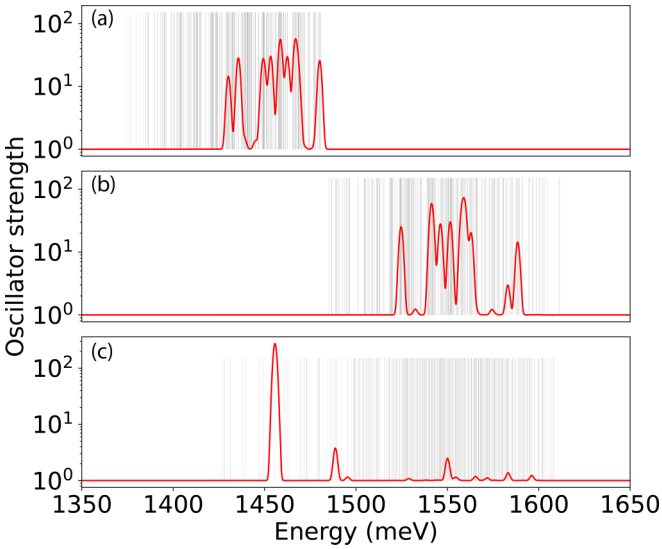

FIG. 5. Low-energy absorption spectrum for a quantum dot (QD) with $R_{\mathrm{QD}} = 20\,\mathrm{nm}$, $V_0 = 100\,\mathrm{meV}$, and $\epsilon = 3.9$. (a) shows the single-particle picture, (b) includes self-energy and vertex corrections on top of it, and (c) also allows for the scattering of configurations. The broadening has been added by hand.

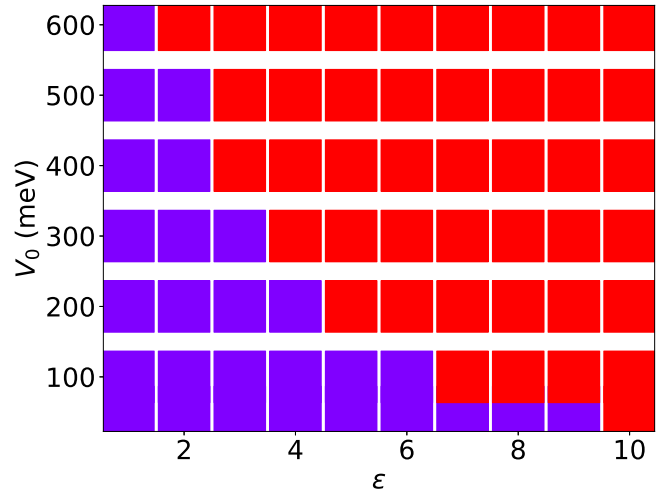

FIG. 6. Color map showing in purple the regions in the parameter space V_0 vs ϵ where the transition to a localized electron state has lower energy than the transition to a delocalized one.

Figure 5 shows the absorption spectrum of the QD as a function of the photon frequency. The red line represents the absorption strength for the active transitions, while the vertical black lines correspond to all excitonic energies.

The upper panel shows the noninteracting excitation spectrum. In this situation, there are more peaks than for the auxiliary QD since the potential correction created mixing between different shells of the auxiliary QD.

In the center panel, we include the effect of electron-hole interaction, without yet considering scattering between different excitonic configurations. Note that the Coulomb interaction produced a blueshift in the energy in the same way as in the auxiliary QD.

The lower panel in Fig. 5 displays the absorption spectrum of the exciton, including all terms in the electron-electron interaction matrix elements. Here, we again observe a redistribution of peak heights, given by correlations between different excitonic configurations. Additionally, the brightest peak experiences a redshift after including the correlation between different exciton configurations.

As discussed previously and illustrated schematically in Fig. 2, the energy of bound electron-hole pairs can be lower than those of localized holes and delocalized electrons, depending on the competition between the electron repelling potential and the electron-hole attraction. One can estimate the energy of the type-II excitation, in which the hole is inside the QD and the electron is outside, by considering the energy required to remove one electron from the highest VB states and place it in the lowest CB state that is delocalized. This transition energy is given by

$$E^*_{\mathrm{ex}} = E_g - E_{-1} + \frac{1}{\epsilon}\sum_{k\in\mathrm{VB}} V_{-1,k,-1,k}\delta_{\sigma_{-1},\sigma_k}. \qquad (18)$$

Here, E_g represents the material gap energy, E_{-1} denotes the energy of the highest-energy hole state, measured from the top of the VB, and the last term accounts for the self-energy of this state, which includes interactions with the positive background and exchange interactions with the filled VB states.

Figure 6 shows in the parameter space V_0 vs ϵ, the region, represented by purple color, in which the energy of the lowest bright transition is lower than the energy of transition from a localized hole state to a bulk CB state. Note that the optimal situation, i.e., exciton is confined, when the interaction is strong (small ϵ) and the confinement is weak (small V_0). For $V_0 = 100\,\mathrm{meV}$, the situation studied previously, the transition to a localized excitation has lower energy than the delocalized one for dielectric constants $\epsilon < 7$. A similar qualitative dependency was observed for a type-II self-assembled QD in Ref. [60], in which changing the barrier potential for holes resulted in competition between lowest-energy type-I and II excitons obtained using effective mass approximation.

IV. CONCLUSIONS

We have presented a theory of excitons confined in gated WSe_2 QDs. In this paper, we address the nontrivial challenge of confining excitons in gated QDs, where holes are attracted but the gate potential repels electrons. For an exciton to exist in a quantum dot, the repulsion of electrons by the gate potential must be balanced with the attraction by the Coulomb potential of a hole localized within the dot. Excitons can be successfully confined within the QD through a delicate interplay of these forces, enabling their detection via transport experiments.

We described our WSe_2 QD using a computational box containing >1 million atoms and employing a tight-binding microscopic Hamiltonian. By applying gates to create a confining potential, attractive for holes and repulsive for electrons, we obtained QD energy levels and wave functions by expanding the QD wave function in bulk band states.

Subsequently, we split our Hamiltonian into an auxiliary Hamiltonian and a perturbation. The auxiliary Hamiltonian confined both electrons and holes. We obtained the excitonic states of the auxiliary QD and expanded the excitonic states of

the true QD in this auxiliary basis. In this basis, the repulsive potential of the gate pulled only the electron in the CB away from the QD but localized the VB hole. This approach enabled us to predict a set of parameters for which excitons are trapped in gated QDs in 2D materials and can be detected using transport.

ACKNOWLEDGMENTS

This paper was supported by the Quantum Sensors Challenge Program QSP-078, High Throughput Networks HTSN-341, and Applied Quantum Computing AQC-004 Challenge Programs at the National Research Council of Canada, NSERC Discovery Grant No. RGPIN-2019-05714, NSERC Alliance Quantum Grant No. ALLRP/578466-2022, and University of Ottawa Research Chair in Quantum Theory of Materials, Nanostructures, and Devices. M.B. acknowledges financial support from the National Science Centre, Poland, under Grant No. 2021/43/D/ST3/01989. This paper was partly enabled by support provided by the Digital Research Alliance of Canada [61].

[1] M. Ciorga, A. S. Sachrajda, P. Hawrylak, C. Gould, P. Zawadzki, S. Jullian, Y. Feng, and Z. Wasilewski, Addition spectrum of a lateral dot from Coulomb and spin-blockade spectroscopy, Phys. Rev. B **61**, R16315 (2000).

[2] T. Fujita, K. Morimoto, H. Kiyama, G. Allison, M. Larsson, A. Ludwig, S. R. Valentin, A. D. Wieck, A. Oiwa, and S. Tarucha, Angular momentum transfer from photon polarization to an electron spin in a gate-defined quantum dot, Nat. Commun. **10**, 2991 (2019).

[3] A. Pioda, E. Totoki, H. Kiyama, T. Fujita, G. Allison, T. Asayama, A. Oiwa, and S. Tarucha, Single-shot detection of electrons generated by individual photons in a tunable lateral quantum dot, Phys. Rev. Lett. **106**, 146804 (2011).

[4] G. J. Schinner, J. Repp, E. Schubert, A. K. Rai, D. Reuter, A. D. Wieck, A. O. Govorov, A. W. Holleitner, and J. P. Kotthaus, Confinement and interaction of single indirect excitons in a voltage-controlled trap formed inside double InGaAs quantum wells, Phys. Rev. Lett. **110**, 127403 (2013).

[5] J. Boddison-Chouinard, A. Bogan, N. Fong, K. Watanabe, T. Taniguchi, S. Studenikin, A. Sachrajda, M. Korkusinski, A. Altintas, M. Bieniek *et al.*, Gate-controlled quantum dots in monolayer WSe_2, Appl. Phys. Lett. **119**, 133104 (2021).

[6] J. Boddison-Chouinard, A. Bogan, P. Barrios, J. Lapointe, K. Watanabe, T. Taniguchi, J. Pawłowski, D. Miravet, M. Bieniek, P. Hawrylak *et al.*, Anomalous conductance quantization of a one-dimensional channel in monolayer WSe_2, npj 2D Mater. Appl. **7**, 50 (2023).

[7] E. S. Kadantsev and P. Hawrylak, Electronic structure of a single MoS_2 monolayer, Solid State Commun. **152**, 909 (2012).

[8] K. E. J. Goh, F. Bussolotti, C. S. Lau, D. Kotekar-Patil, Z. E. Ooi, and J. Y. Chee, Toward valley-coupled spin qubits, Adv. Quantum Technol. **3**, 1900123 (2020).

[9] J. F. Sierra, J. Fabian, R. K. Kawakami, S. Roche, and S. O. Valenzuela, Van der Waals heterostructures for spintronics and opto-spintronics, Nat. Nanotechnol. **16**, 856 (2021).

[10] A. Splendiani, L. Sun, Y. Zhang, T. Li, J. Kim, C.-Y. Chim, G. Galli, and F. Wang, Emerging photoluminescence in monolayer MoS_2, Nano Lett. **10**, 1271 (2010).

[11] J. G. Roch, G. Froehlicher, N. Leisgang, P. Makk, K. Watanabe, T. Taniguchi, and R. J. Warburton, Spin-polarized electrons in monolayer MoS_2, Nat. Nanotechnol. **14**, 432 (2019).

[12] T. Scrace, Y. Tsai, B. Barman, L. Schweidenback, A. Petrou, G. Kioseoglou, I. Ozfidan, M. Korkusinski, and P. Hawrylak, Magnetoluminescence and valley polarized state of a two-dimensional electron gas in WS_2 monolayers, Nat. Nanotechnol. **10**, 603 (2015).

[13] D. Van Tuan, A. M. Jones, M. Yang, X. Xu, and H. Dery, Virtual trions in the photoluminescence of monolayer transition-metal dichalcogenides, Phys. Rev. Lett. **122**, 217401 (2019).

[14] H.-P. Komsa and A. V. Krasheninnikov, Two-dimensional transition metal dichalcogenide alloys: Stability and electronic properties, J. Phys. Chem. Lett. **3**, 3652 (2012).

[15] T. Mueller and E. Malic, Exciton physics and device application of two-dimensional transition metal dichalcogenide semiconductors, npj 2D Mater. Appl. **2**, 29 (2018).

[16] C. Schneider, M. M. Glazov, T. Korn, S. Höfling, and B. Urbaszek, Two-dimensional semiconductors in the regime of strong light-matter coupling, Nat. Commun. **9**, 2695 (2018).

[17] H. J. Conley, B. Wang, J. I. Ziegler, R. F. Haglund Jr, S. T. Pantelides, and K. I. Bolotin, Bandgap engineering of strained monolayer and bilayer MoS_2, Nano Lett. **13**, 3626 (2013).

[18] S. Manzeli, D. Ovchinnikov, D. Pasquier, O. V. Yazyev, and A. Kis, 2D transition metal dichalcogenides, Nat. Rev. Mater. **2**, 17033 (2017).

[19] A. H. Castro Neto, F. Guinea, N. M. R. Peres, K. S. Novoselov, and A. K. Geim, The electronic properties of graphene, Rev. Mod. Phys. **81**, 109 (2009).

[20] K. F. Mak, C. Lee, J. Hone, J. Shan, and T. F. Heinz, Atomically thin MoS_2: A new direct-gap semiconductor, Phys. Rev. Lett. **105**, 136805 (2010).

[21] M. Bieniek, M. Korkusiński, L. Szulakowska, P. Potasz, I. Ozfidan, and P. Hawrylak, Band nesting, massive Dirac fermions, and valley Landé and Zeeman effects in transition metal dichalcogenides: A tight-binding model, Phys. Rev. B **97**, 085153 (2018).

[22] A. Altıntaş, M. Bieniek, A. Dusko, M. Korkusiński, J. Pawłowski, and P. Hawrylak, Spin-valley qubits in gated quantum dots in a single layer of transition metal dichalcogenides, Phys. Rev. B **104**, 195412 (2021).

[23] M. Bieniek, L. Szulakowska, and P. Hawrylak, Effect of valley, spin, and band nesting on the electronic properties of gated quantum dots in a single layer of transition metal dichalcogenides, Phys. Rev. B **101**, 035401 (2020).

[24] D. Miravet, A. Altıntaş, A. W. Rodrigues, M. Bieniek, M. Korkusinski, and P. Hawrylak, Interacting holes in gated WSe_2 quantum dots, Phys. Rev. B **108**, 195407 (2023).

[25] K. He, N. Kumar, L. Zhao, Z. Wang, K. F. Mak, H. Zhao, and J. Shan, Tightly bound excitons in monolayer WSe_2, Phys. Rev. Lett. **113**, 026803 (2014).

[26] Y. Otsuka, S. Yunoki, and S. Sorella, Universal quantum criticality in the metal-insulator transition of two-dimensional interacting Dirac electrons, Phys. Rev. X **6**, 011029 (2016).

[27] M. Bieniek, K. Sadecka, L. Szulakowska, and P. Hawrylak, Theory of excitons in atomically thin semiconductors: Tight-binding approach, Nanomaterials **12**, 1582 (2022).

[28] H. S. Borges, C. A. N. Júnior, D. S. Brandão, F. Liu, V. V. R. Pereira, S. J. Xie, F. Qu, and A. M. Alcalde, Persistent entanglement of valley exciton qubits in transition metal dichalcogenides integrated into a bimodal optical cavity, Phys. Rev. B **107**, 035404 (2023).

[29] F. Wu, F. Qu, and A. H. MacDonald, Exciton band structure of monolayer MoS_2, Phys. Rev. B **91**, 075310 (2015).

[30] M. Goryca, J. Li, A. V. Stier, T. Taniguchi, K. Watanabe, E. Courtade, S. Shree, C. Robert, B. Urbaszek, X. Marie *et al.*, Revealing exciton masses and dielectric properties of monolayer semiconductors with high magnetic fields, Nat. Commun. **10**, 4172 (2019).

[31] D. Thureja, A. Imamoglu, T. Smoleński, I. Amelio, A. Popert, T. Chervy, X. Lu, S. Liu, K. Barmak, K. Watanabe *et al.*, Electrically tunable quantum confinement of neutral excitons, Nature (London) **606**, 298 (2022).

[32] D. Thureja, F. E. Yazici, T. Smolenski, M. Kroner, D. J. Norris, and A. Imamoglu, Electrically defined quantum dots for bosonic excitons, arXiv:2402.19278v2.

[33] D. Le, A. Barinov, E. Preciado, M. Isarraraz, I. Tanabe, T. Komesu, C. Troha, L. Bartels, T. S. Rahman, and P. A. Dowben, Spin-orbit coupling in the band structure of monolayer WSe_2, J. Phys.: Condens. Matter **27**, 182201 (2015).

[34] N. Alidoust, G. Bian, S.-Y. Xu, R. Sankar, M. Neupane, C. Liu, I. Belopolski, D.-X. Qu, J. D. Denlinger, F.-C. Chou *et al.*, Observation of monolayer valence band spin-orbit effect and induced quantum well states in MoX_2, Nat. Commun. **5**, 4673 (2014).

[35] A. D. Güçlü, P. Potasz, M. Korkusinski, and P. Hawrylak, *Graphene Quantum Dots* (Springer, Berlin, 2014).

[36] J. Güttinger, T. Frey, C. Stampfer, T. Ihn, and K. Ensslin, Spin states in graphene quantum dots, Phys. Rev. Lett. **105**, 116801 (2010).

[37] J. A. McGuire, Growth and optical properties of colloidal graphene quantum dots, Phys. Status Solidi **10**, 91 (2016).

[38] S. Wang, N. Kharche, E. Costa Girão, X. Feng, K. Müllen, V. Meunier, R. Fasel, and P. Ruffieux, Quantum dots in graphene nanoribbons, Nano Lett. **17**, 4277 (2017).

[39] K. Wang, K. De Greve, L. A. Jauregui, A. Sushko, A. High, Y. Zhou, G. Scuri, T. Taniguchi, K. Watanabe, M. D. Lukin *et al.*, Electrical control of charged carriers and excitons in atomically thin materials, Nat. Nanotechnol. **13**, 128 (2018).

[40] R. Pisoni, Z. Lei, P. Back, M. Eich, H. Overweg, Y. Lee, K. Watanabe, T. Taniguchi, T. Ihn, and K. Ensslin, Gate-tunable quantum dot in a high quality single layer MoS_2 van der Waals heterostructure, Appl. Phys. Lett. **112**, 123101 (2018).

[41] C. Volk, S. Fringes, B. Terrés, J. Dauber, S. Engels, S. Trellenkamp, and C. Stampfer, Electronic excited states in bilayer graphene double quantum dots, Nano Lett. **11**, 3581 (2011).

[42] M. T. Allen, J. Martin, and A. Yacoby, Gate-defined quantum confinement in suspended bilayer graphene, Nat. Commun. **3**, 934 (2012).

[43] M. Eich, F. Herman, R. Pisoni, H. Overweg, A. Kurzmann, Y. Lee, P. Rickhaus, K. Watanabe, T. Taniguchi, M. Sigrist, T. Ihn, and K. Ensslin, Spin and valley states in gate-defined bilayer graphene quantum dots, Phys. Rev. X **8**, 031023 (2018).

[44] A. Kurzmann, M. Eich, H. Overweg, M. Mangold, F. Herman, P. Rickhaus, R. Pisoni, Y. Lee, R. Garreis, C. Tong *et al.*, Excited states in bilayer graphene quantum dots, Phys. Rev. Lett. **123**, 026803 (2019).

[45] N. M. Freitag, L. A. Chizhova, P. Nemes-Incze, C. R. Woods, R. V. Gorbachev, Y. Cao, A. K. Geim, K. S. Novoselov, J. Burgdörfer, F. Libisch *et al.*, Electrostatically confined monolayer graphene quantum dots with orbital and valley splittings, Nano Lett. **16**, 5798 (2016).

[46] Y. Saleem, K. Sadecka, M. Korkusinski, D. Miravet, A. Dusko, and P. Hawrylak, Theory of excitons in gated bilayer graphene quantum dots, Nano Lett. **23**, 2998 (2023).

[47] S. Davari, J. Stacy, A. M. Mercado, J. D. Tull, R. Basnet, K. Pandey, K. Watanabe, T. Taniguchi, J. Hu, and H. O. H. Churchill, Gate-defined accumulation-mode quantum dots in monolayer and bilayer WSe_2, Phys. Rev. Appl. **13**, 054058 (2020).

[48] M. Brotons-Gisbert, A. Branny, S. Kumar, R. Picard, R. Proux, M. Gray, K. S. Burch, K. Watanabe, T. Taniguchi, and B. D. Gerardot, Coulomb blockade in an atomically thin quantum dot coupled to a tunable Fermi reservoir, Nat. Nanotechnol. **14**, 442 (2019).

[49] X. Lu, X. Chen, S. Dubey, Q. Yao, W. Li, X. Wang, Q. Xiong, and A. Srivastava, Optical initialization of a single spin-valley in charged WSe_2 quantum dots, Nat. Nanotechnol. **14**, 426 (2019).

[50] C. Chakraborty, L. Qiu, K. Konthasinghe, A. Mukherjee, S. Dhara, and N. Vamivakas, 3D localized trions in monolayer WSe_2 in a charge tunable van der Waals heterostructure, Nano Lett. **18**, 2859 (2018).

[51] Z.-Z. Zhang, X.-X. Song, G. Luo, G.-W. Deng, V. Mosallanejad, T. Taniguchi, K. Watanabe, H.-O. Li, G. Cao, G.-C. Guo *et al.*, Electrotunable artificial molecules based on van der Waals heterostructures, Sci. Adv. **3**, e1701699 (2017).

[52] S. Bhandari, K. Wang, K. Watanabe, T. Taniguchi, P. Kim, and R. Westervelt, Imaging quantum dot formation in MoS_2 nanostructures, Nanotechnology **29**, 42LT03 (2018).

[53] Q. Chen, L. L. Li, and F. M. Peeters, Magnetic field dependence of electronic properties of MoS_2 quantum dots with different edges, Phys. Rev. B **97**, 085437 (2018).

[54] L. Szulakowska, M. Cygorek, M. Bieniek, and P. Hawrylak, Valley- and spin-polarized broken-symmetry states of interacting electrons in gated MoS_2 quantum dots, Phys. Rev. B **102**, 245410 (2020).

[55] J. Pawłowski, M. Bieniek, and T. Woźniak, Valley two-qubit system in a MoS_2-monolayer gated double quantum dot, Phys. Rev. Appl. **15**, 054025 (2021).

[56] M. Korkusinski, Y. Saleem, A. Dusko, D. Miravet, and P. Hawrylak, Spontaneous spin and valley symmetry-broken states of interacting massive Dirac fermions in a bilayer graphene quantum dot, Nano Lett. **23**, 7546 (2023).

[57] J. Pawłowski, D. Miravet, M. Bieniek, M. Korkusinski, J. Boddison-Chouinard, L. Gaudreau, A. Luican-Mayer, and P. Hawrylak, Interacting holes in a gated WSe_2 quantum channel: Valley correlations and zigzag Wigner crystal, Phys. Rev. B **110**, 125147 (2024).

[58] G. Wang, X. Marie, I. Gerber, T. Amand, D. Lagarde, L. Bouet, M. Vidal, A. Balocchi, and B. Urbaszek, Giant enhancement of the optical second-harmonic emission of WSe_2 monolayers by laser excitation at exciton resonances, Phys. Rev. Lett. **114**, 097403 (2015).

[59] X.-X. Song, D. Liu, V. Mosallanejad, J. You, T.-Y. Han, D.-T. Chen, H.-O. Li, G. Cao, M. Xiao, G.-C. Guo *et al.*, A gate defined quantum dot on the two-dimensional transition metal dichalcogenide semiconductor WSe_2, Nanoscale **7**, 16867 (2015).

[60] K. L. Janssens, B. Partoens, and F. M. Peeters, Magnetoexcitons in planar type-II quantum dots in a perpendicular magnetic field, Phys. Rev. B **64**, 155324 (2001).

[61] www.alliancecan.ca.